Severity Assessment of Aircraft Engine Fan Blades under Airborne Collision of Unmanned Aerial Vehicles Comparable to Bird Strike Certification Standards

Mohd Hasrizam Che Man [1], Hu Liu [1] and Kin Huat Low [2]

Abstract

Airborne drone collision on commercial manned aircraft has received extensive awareness due to the increasing drone operations in the restricted airspace. In addition, the bird strike certification for aircraft engines is likely to be inadequate for a drone collision with identical kinetic energy due to the difference in damage levels. Thus, it is important to understand and compare the risk between drones and bird strikes. This study aims to understand the damage severity from bird and drone strikes on the manned commercial aircraft engine. The Finite Element Method (FEM) simulation is adopted to obtain the damage of engine fan blades under the drone collision and bird strikes at different collision positions. The Lagrangian and Smooth Particle Hydrodynamics (SPH) approaches are employed for the drone and bird simulations, respectively. In addition, three different drone and bird weight categories were considered in this study, namely small, medium, and large, to investigate the effect of kinetic energy on the damage of fan blades. Results from the FEM simulation demonstrated that the damage of the engine fan blades due to drone collisions were more severe when comparing bird strikes of the same weight category. The damage severity level was proposed based on the damage of engine fan blades. In the event of a drone ingestion, the damage severity level assists in the identification of potential damage to engine fan blades and its performance.

Keywords: Bird strike, drone collision, engine ingestion, SPH, damage severity level.

Nomenclature

CAD	Computer Aided Design
FEM	Finite Element Method
FOD	Foreign Object Damage
HPC	High-Pressure Compressor

[1] Air Traffic Management Research Institute (ATMRI), Nanyang Technological University (NTU), Singapore, 637460.
[2] School of Mechanical and Aerospace Engineering, Nanyang Technological University, Singapore, 639798.

Corresponding author: Kin Huat Low, School of Mechanical and Aerospace Engineering, Nanyang Technological University, Singapore, 639798
e-mail: mkhlow@ntu.edu.sg

LPC Low-Pressure Compressor
SPH Smooth Particle Hydrodynamics
UAVs Unmanned Aerial Vehicles

1. Introduction

It is estimated that by the year 2020, the number of UAVs (or drones) over the world will reach 4.7 million units [1], which would lead to significant threats for the safety management of manned aircraft operation [2]. Many cases of unauthorized drones intruded into restricted airspace like airport area, such as the drone incident in Gatwick airport in December 2018 [3]. However, due to unclear risk posed by the unauthorized drones in the airport area, the common measure taken by airport management is shutting down the runway operation, which may disrupt the airport operation and even result in diversion, delay, and cancellation of flights [4-6]. Hence, it is urgent to present a method to evaluate aircraft damage level caused by UAV (unmanned aerial vehicle) airborne collision [7].

In the past few decades, the bird has been one of the threats to commercial aircraft operation, which has caused damage of aircraft structure [8-13] and lead to 258 fatalities from the aircraft crash during the year of 1988-2014 [14]. Due to concern on this issue, many works have been done to evaluate the damage severity of bird strikes on commercial aircraft engine [15], wing leading edge [16, 17], and windshield [18, 19]. At the same time, a lot of certification standards have been developed within these few decades to enhance the safety and efficiency of aircraft operation.

The FAA and EASA have established bird certification for engine ingestions caused by different weights of birds. Current standards are applied to engine ingestion for both multiple and single bird ingestions into a single fixed-wing aircraft engine as established in 14 CFR Part 33-77 by FAA and 'Bird Strike and Ingestion' in EASA Airworthiness Code CS-E 800 [20]. In outline, the standards required the engine has to be proved by testing for an initial climb and take-off flight phase where single bird ingestion with a maximum weight between 1.8 kg and 3.65 kg into the engine inlet area shall not cause an engine to suffer an uncontained failure and shall maintain at least 50% thrust without losing the capability to shut down the engine after ingestion [20]. However, the engine fan blades is a crucial risk area because it the main component to produce thrust, and any damage may cause partial or complete loss of thrust, which might lead to out of balance forces (windmill) and may cause further damage the whole engine structural integrity [21]. The bird strike is an aircraft certification standard required for the aircraft to withstand and continue flight without sudden damage to the engine (e.g.,

thrust loss) after the bird strike occurs. However, currently, no certification for drone collision with an aircraft engine has been fully established.

A report by CAA [7] has identified the risk of a drone collision with large passenger aircraft for a drone weight under 2 kg is a prime concern, mainly because of the number of passengers involved in the accident and because these aircraft often fly over densely populated urban areas [7]. Although the likelihood of encounters between small (2 kg or less) drones and other air traffic is increasing [22], the potential risk to aircraft for drone size larger than 2 kg is also a crucial task to understand damage severity level which can be used for safety requirement of the large passenger aircraft certification. However, this study focuses only on the drones with their weight larger than 2 kg, and the damage severity caused by different weight categories of drones still needs careful analysis.

Few studies have carried out to reveal the damage to aircraft caused by drone collision. For example, the drone collision study impacted the aircraft wings and vertical stabilizers by Olivares et al. [23, 24]. Investigations by Lu et al. [25] of drone impact onto a windshield of commercial aircraft to reveal the influence of pitch and yaw angles of UAVs on the damage of windscreen. However, the research on drone collision to aircraft engines is very limited. Pioneering work on this topic was carried out by D'Souza et al. [26] to study drone collisions on a generic commercial manned aircraft engine, which suggested that drone collisions may cause more significant damage to aircraft structure than bird strikes for the equivalent impact energy level. Most damage from drone collision is produced by the stiffer components of the drone (e.g. motor, camera and battery) compared to a bird strike [20]. However, in their study, they only considered a multi-rotor drone category with a weight under 2 kg. Therefore, a comparison of damage between for bird and drone with weight more than 2 kg is important to better understand the damage severity of the drone collision to large passenger aircraft.

A lot of risk assessment method for evaluation of bird collision in the airport area has been developed. For example, the Aviation Safety Ranking Value (ASRV) was suggested by the International Bird Strike Committee (IBSC) [27] to evaluate and classify the risk pose by particular bird species due to bird strikes. This ranking represents the risk of birds strike into five levels based on the potential impact and cost to aircraft [28]. The level in the ranking is assessed based on the size (mainly weight) of each particular birds, the moving pattern and activities of the birds in the airport [29], which are defined

as follows: Level 1 means no significant impact on air traffic safety, Level 2 stands for low potential danger, Level 3 is intermediate potential danger; Level 4 denotes potential severe danger, while Level 5 indicates very high potential danger [29]. It worth to be noted that the risk assessment is mainly established from the bird strike database, which is different than drone collision because very limited collision data available in database, therefore the drone collision simulation on aircraft engine could provide insight on possible damage severity of aircraft engine under the drone collision.

Researchers also have proposed a rapid assessment method to identify the potential risk of the bird strike for a specific bird and precautionary action to be taken using the species-specific bird strike risk index (SSBR) [30]. A study by Liu et al. [31] revealed that the drone weight of 750 g could cause large deformation to engine fan blades. Study the impact of large drone category on aircraft engine by Hasrizam et al., [32] have reported the damage caused to engine low-pressure compressor (LPC) and high-pressure compressor (HPC), may lead to thrust loss up to 75%. Nevertheless, to the author's knowledge, no comprehensive damage severity assessment tool has been proposed to evaluate the potential risk level of drone intrusion into airport airspace and to air traffic safety. Several issues remain to be understood the risk of drone engine ingestion. The novelty of our study is listed as follows:

- Compare damage of bird strike and drone collisions on the aircraft engine fan blades for different weight categories equivalent to bird strike certification standards.
- Different real drone model categories were developed for engine ingestion FEM simulation.
- Establish a damage severity assessment for the airborne collision between UAVs and manned aircraft engine fan blades considering the influence of various collision parameters.

The outline of this paper is presented as follows: The first section is the introduction of the bird certification requirement, and risk assessment for bird collision is presented to be compared with drone collision. Section two is the methodology of analysis, which include weight category of drone and bird considered in this study the simulation parameters and damage severity level definition. Next is the simulation setups, including the material properties of drone, birds and engine presented in section 3. Validation of simulation works with experimental results for birds and fan blades material

properties and comparing the damage severity of engine fan blades under bird strike, and drone collision is presented in section four. Section 5 has presented the simulation results of the drone collision parametric study for different impact velocities, engine rotation speed and impact position and summarized the simulation results by comparing the damage severity of engine fan blades under the bird drone collision for different weight categories. Finally, several conclusions drawn from the study presented in the last section.

2. Methodology of Analysis

To investigate the influence of a bird strike and drone collision on aircraft engine fan blades, firstly, a FEM simulation model of three different weight categories of bird and drone impacting onto engine fan blades will be carefully established by using a commercially available code, ABAQUS/Explicit[33] . Secondly, the impact parameter like engine rotation speed, collision inclination angle, collision velocity and collision position will be investigated in detail in this study. Lastly, the definition of damage level on the engine fan blades from the collision with the different bird and drone categories will be presented.

2.1. Drone and Bird Categories

Foreign object damage (FOD) threats the main interest in the present study existing mainly during low altitude flight phases, such as take-off, climb and approach [26] caused by bird strike and drone collision. Several birds and drone categories are selected to assess the damage severity of the engine fan blades to the bird strike and drone collision, as shown in Table 1. Three different birds and drones have been selected to represent each category; namely, small, medium, and large sizes with the tip-to-tip dimensions (length x width x height) for small, medium, and large drone has the size of 159 x 202 x 55 mm, 290 x 290 x 196 mm, and 437 x 302 x 453 mm, respectively.

Table 1 Categorization for birds and drones.

Bird [34]		**Drone [35]**	
Category	**Weight (kg)**	**Category**	**Weight (kg)**
Small	<1.85	Small*	0.25-1.5
Medium	1.85-3.65	Medium	1.5-3.5
Large	>3.65	Large	>3.5

*Drone weight less than250g is categorized as harmless.

Figure 1 shows the 3D CAD drawing of the drone generated in this study for different drone categories and material type of every drone component. Three drones represent three different weight categories with 249 g, 1280 g and 3200 g for small, medium and large drones, respectively, which are comparable to bird strike certification requirement[34].

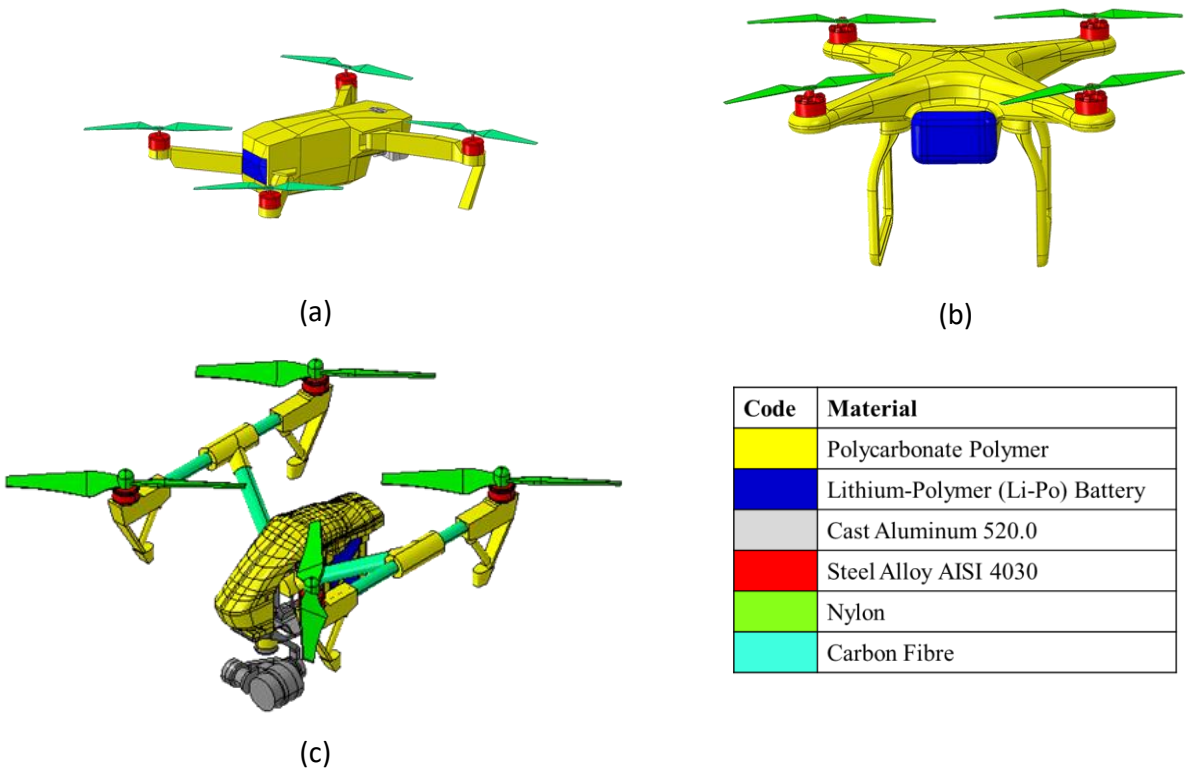

Figure 1 FEM model and material distribution of (a) MAVIC MINI, (b) Phantom 3, and (c) Inspire 1.

2.2 Impact Case Parameters

It is worth noting that the bird may be considered soft body impacts where the response of the impactor characterized as hydrodynamic, which can be modelled using SPH in FEM simulation. The drone motor, battery, and camera can be considered the hard body since their material strengths are significantly higher than the bird; hence, the stresses developed during the drone collision can be solved using the Lagrangian method with the aid of FEM simulation. The impact cases considered in this collision simulation for bird and drone are summarized in Table 2. Figure 2(a) shows a diagram of different drone's collision positions on engine fan blades. The impact angle of drone and engine fan blades is taken as 10°, which is depicted in Figure 2(b) to represent the maximum angle during the

take-off flight phase where most of the collision is expected to happen at this height and caused most severe damage to the aircraft engine[36].

Table 2 Impact case parameter.

Impactors	Parameters			
	Impact Velocity (Relative) [37]	**Engine Rotation** [38]	**Impact Angle (Inclination)** [39]	**Collision Position**
Bird	145, 200, 250 knots	3000, 4000, 5000RPM	10°	25%, 50% and 75%
Drone	145 knots	5000RPM	10°	25%, 50% and 75%

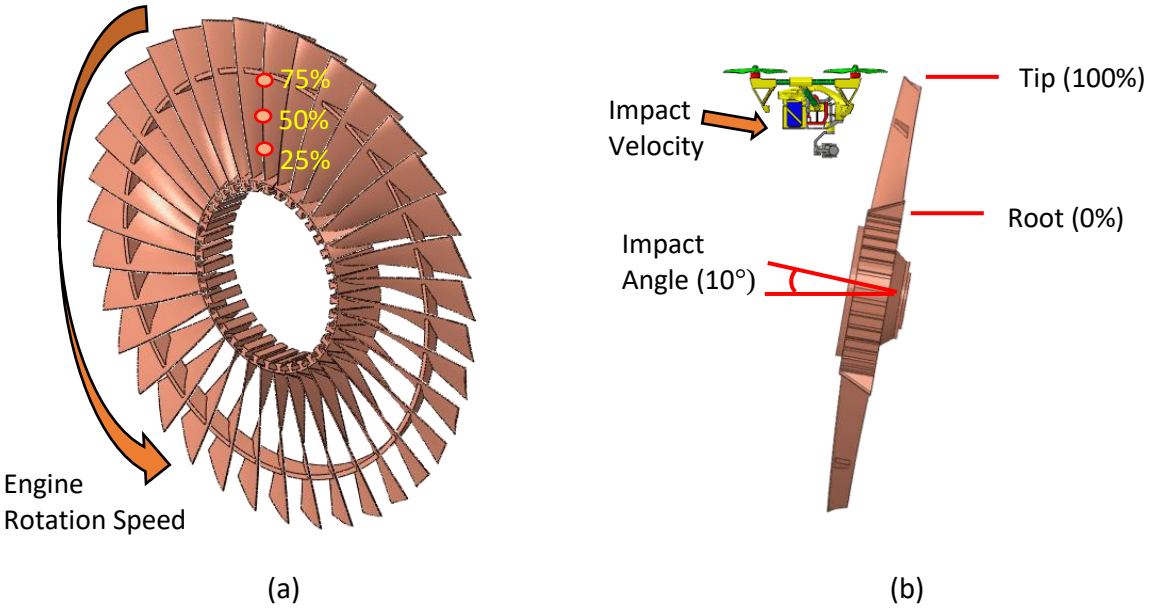

Figure 2 Simulation case parameters (a) isometric view of collision position; (b) side view of the collision position of 75% at impact angle 10°.

2.3 Definition of Damage Severity Level

Collision for bird and drone onto engine fan blades may inflict different levels of damage severity. The results of the damage severity level presented in this paper are based on the assumptions that the FEM computational model provides a reliable simulation of the events occurring during impact and contact at several points during the collision process. In addition, the simulation also includes an impact of a projectile with the engine with several contact points of structures with apart stiffness and strengths.

The details for the definition of damage severity level are exhibited in Table 3, where the damage level is based on how much engine to produce power and aircraft can be controlled for a safe emergency landing in case of bird strike took places[26]. In damage level 1, the impact on the fan blade only causes slight damage to engine fan blade, like nick. In damage severity level 4, the damage due to the impact can be very severe where severe fan blades fractured[40], which will lead to the total loss of thrust and imbalance force [41] and finally cause the loss of engine integrity.

Table 3 Description of fan blades damage severity level assessment.

Damage Level	Description
Level 1	No significant damage to the fan blade (e.g., small indentation).
Level 2	Slight damage to the fan blade (e.g., small bending or small material loss).
Level 3	Damage to fan blade (e.g., large bending, large material loss or tear).
Level 4	Severe damage to fan blade (e.g., Fan blade fractured).

3. Parameters and Material Properties for FEM Simulation

In this study, the FEM simulation is employed in this work is to assess the damage severity from the collision of bird and drone with aircraft engine fan blades. In this section, we will discuss the FEM simulation parameters and material properties and material model because this analysis involves a projectile that has parts from a combination of low and high stiffness that behave differently under impact load and requires careful consideration. Different material properties used for bird, drone, and aircraft engine fan blades and mesh sizing and interaction behavior are also presented in this section.

3.1. Drone Model

The material properties of drones used in the collision simulation correspond to those different materials, namely polycarbonate, lithium-polymer, aluminium, steel, nylon, and carbon fiber (only Inspire 1). Table 4 lists a summary of the material properties used for the drone model in the FEM simulation.

All materials in the simulation are described by an elastic-plastic stress-strain relation with a simple ultimate stress failure criterion. Such assumption is valid as long contact time is very long as

most of the drone parts are soft material. Hence, the impact has a long time to distribute the impact force into a larger contact area that simple stress failure without strain-rate effect is sufficient to predict damage of the drone's structures.

Table 4 Material Properties of Drone.

Materials	**Properties**					
	Density, ρ	**Young's Modulus, E**	**Poison's ratio, υ**	**Yield stress, σ_y**	**Failure stress, σ_f**	**Failure strain, ε_f**
Polycarbonate Polymer [26]	1197.8 kg/m^3	2.59 GPa	0.37	50 MPa	50 MPa	0.50
Lithium-Polymer [42]	1755 kg/m^3	500 MPa	0.01	30 MPa	55 MPa	0.375
Aluminium [43]	2600 kg/m^3	66 GPa	0.33	170 MPa	330 MPa	0.140
Steel 4030 [44]	7800 kg/m^3	210 GPa	0.30	-	-	-
Nylon [26]	1340 kg/m^3	2.20 GPa	0.42	105 MPa	130 MPa	0.25
Carbon Fibre [45]	1590 kg/m^3	135 GPa	0.32	2,207 MPa	2,207 MPa	0.0145

The damage model for the rest of the drone and engine parts is made from polymer and lithium-polymer, which is a fragile material that is often treated as elastic-plastic material, especially in high-speed impact simulation [23, 25].

Only the steel alloy is defined as strain rate dependent, and the dynamic yield stress is approximated by the Johnson-cook relation [46]:

$$\sigma_y = (A + B\varepsilon_p^n)\left[1 + Cln\left(\frac{\dot{\varepsilon}}{\dot{\varepsilon}_o}\right)\right](1 - T^{*m}) \quad (1)$$

where σ_y is the effective stress, and ε_p is the effective plastic strain; $\dot{\varepsilon}$ and $\dot{\varepsilon}_o$ are, respectively, the plastic strain rate and the reference strain rate (usually defined as 1s^{-1}). *A*, *B*, and *n* are the quasi-static yield stress, the initial hardening modulus, and the work hardening coefficient, respectively, which are listed in which are summarized in Table 5.

Table 5 Properties of Johnson-Cook damage for steel alloy [47].

A	**B**	**n**	**m**	**Melting Temperature**
792 MPa	510 MPa	0.26	1.03	1793°C
D1	**D2**	**D3**	**D4**	**D5**
0.05	3.44	-2.12	0.002	0.6

3.2. Engine Model

A medium-sized commercial aircraft engine that is the most used engine for commercial aviation is selected in this study. The inlet region of the turbofan engine considered in this study consists of fan blades, fan disc, nose cone and containment ring, as shown in Figure 3(a). Figure 3(b) and 3(c) are the figure of real fan blades and the 3D CAD drawing of fan blades generated in this study. The external radius is measured from the centerline to the tip of the blade, R_{ex} = 875 mm, and the internal radius is measured to the root of the blade, R_{in} = 330 mm. The fan disc is used to connect between the fan blades and the engine shaft, and the tie constraints behavior is adopted to define this connection type used to connect the fan blades with the fan disc.

The fan blades, fan disc, and shaft of the front engine use Titanium Alloy, Ti-6Al-4V. The containment ring and nose cone is aluminium, with some aluminium honeycomb material in the substrate of the containment ring. The engine structural material properties used in the collision simulation are presented in Table 6. All the structural materials properties used in the simulation are described by an elastic-plastic stress-strain relation with simple ultimate strain failure criterion. The titanium alloy is strain rate dependent (approximated by the Johnson-cook relation), listed in Table *7*.

Table 6 The engine structural Material Properties.

Materials	**Properties**					
	Density, ρ	**Young's Modulus, E**	**Poison's ratio, υ**	**Yield stress, σ_y**	**Failure stress, σ_f**	**Failure strain, ε_f**
Ti-6Al-4V [47]	4430 kg/m^3	1100 GPa	0.33	-	-	-
Aluminium [43]	2600 kg/m^3	66 GPa	0.33	170 MPa	330 MPa	0.14

Table 7 Plastic properties and Johnson-Cook Damage for Titanium Alloy (Ti-6Al-4V) [47].

A	**B**	**n**	**m**	**Melting Temperature**
1098MPa	1092MPa	0.93	1.1	1903°C
D1	**D2**	**D3**	**D4**	**D5**
-0.09	0.25	0.48	0.014	3.87

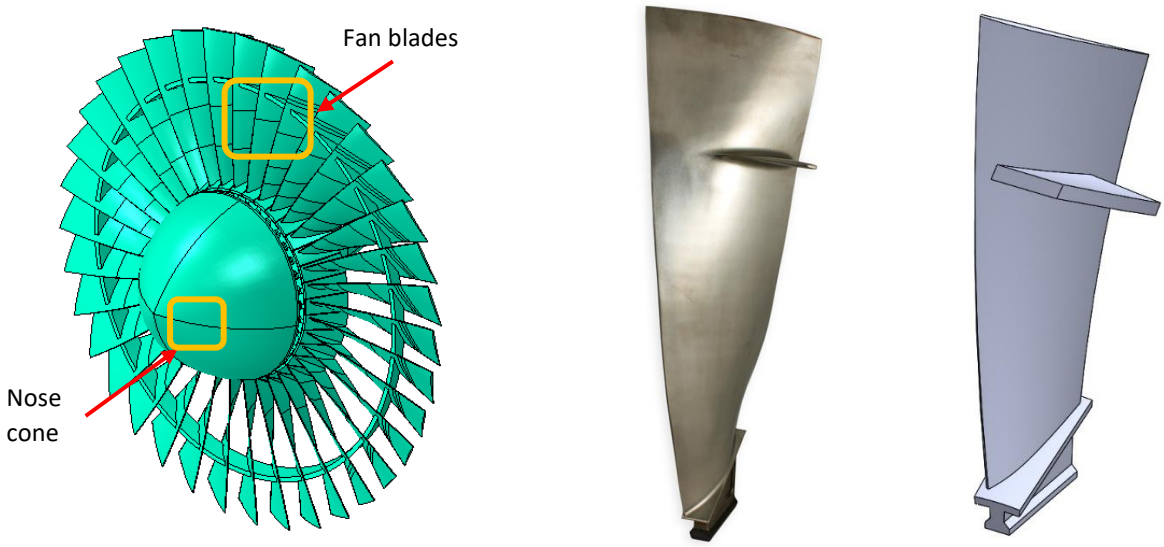

(a) aircraft engine fan blades assembly (b) Real fan blades [48] (c) 3D CAD Drawing

Figure 3 Geometry for aircraft engine model: (a) assembly of aircraft engine fan blades; (b) real fan blades and (c) 3D CAD drawing of fan blades.

3.3. Drone Ingestion Model

As presented in Figure 4, the UAV-engine system combining the aircraft engine and the UAV is assembled for the drone ingestion simulation. The hexahedral element with the C3D8R type is adopted for meshing all the engine parts. The maximum and minimum element sizes for the fan blade used in the simulation are around 1.7 mm and 12.1 mm, respectively. A total number of 944,292 elements are generated for the aircraft engine fan blades assembly. An engine fan blades used for the drone collision simulation contains 6,764 shell elements and 1,031,978 solid elements, with 1,615,536 nodes in total. The mesh size of around twelve fan blades that might have contact with the UAV under the collision is refined for accurate simulation. In Figure 4(b), the first three fan blades are meshed with a graded size in which the contact region has the smallest size presented, and their sizes change gradually from the contact region to the tip and root of the fan blade.

Most of the UAV parts for all three drones are meshed by using hexahedron element with C3D8R type. Besides, some thin-walled structures like the main body and drone arms are meshed as shell element with S4R type. The minimum and maximum element sizes for the main body are 0.75 mm and 2.0 mm, respectively, for the drone of Inspire 1. Furthermore, an average element size of approximately 2.0 to 5.0 mm is adopted to mesh the other parts of the UAV. A total number of

104,928 elements are generated for the UAV model. The detailed FEM model for this UAV is depicted in Figure 4(b). The minimum element sizes for the main body are 1.25 mm and 1.13 mm for MAVIC MINI and Phantom 3, respectively. The main body is meshed with S4R shell elements. For other parts of the UAV, the average element size in a range of 2.0 to 3.0 mm is adopted. The total element number of 192,556 and 169,172 are generated for MAVIC MINI and Phantom 3, respectively.

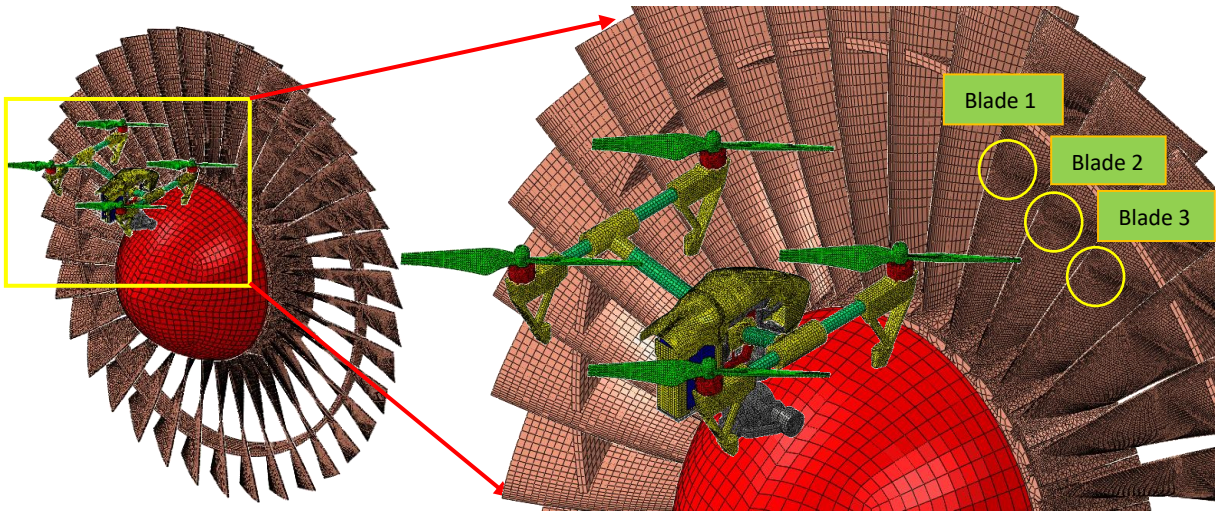

(a) (b)

Figure 4 UAV ingestion simulation model: (a) isometric view for the assembly model of UAV and engine; (b) The engine fan blades refined at the UAV striking position.

The interaction behavior between the engine fan blades and UAV is captured by using a general contact model[33] with a friction coefficient of 0.41[49]. The element-based surface behavior is adopted in the simulation for eroding contact surface, which means the faces can be removed from the contact domain, and the internal exposed faces will be activated once an element is failed. The boundary condition for the simulation is given as follows: fan blades, fan disc, nose cone, and front forward shaft can move rotationally, and the whole engine parts cannot move translationally along the engine rotation axis. The drone propeller rotation is not considered in this study because the relative speed between drone blades and engine rotation is much different, and the rotation of the drone blades is much lower compared to the engine fan blades. Therefore, the rotation of the drone propeller can be neglected.

3.4 Bird Ingestion Model

Apart from drone collision, the bird ingestion will also be compared. The material properties of the bird used in the bird strike simulation correspond to those of gelatin, which possesses similar characteristics and response as a real bird. Figure 5 shows the configurations of the bird model and Table 8 shows its dimension parameters to its corresponding weight category. Table 9 shows summarized the material properties used for the bird model.

Smoothed particle hydrodynamics (SPH) is a meshless Lagrangian technique based on the interpolation theory and smoothing kernel function. The impactor is represented as a set of discrete interacting particles, which are independent of Lagrangian elements. The method provides more accurate results than Lagrangian or Couple Eulerian-Lagrangian (CEL) analysis when the deformation is too severe and can also reduce computational cost.

Figure *6*(**Error! Reference source not found.**a) shows the bird-engine assembly for the bird ingestion model in FEM simulation. Figure *6*(b) shows the SPH model of a bird in this simulation that has 8190 nodes with each node has lumped mass with a weight of 0.1221 g and positioned at an average distance of 5.5 mm between two nodes [50]. In the collision simulations, the aircraft engine is fixed translationally at the front forward shaft with the bird impacted at an initial velocity of 72.5 m/sec with three different collision positions of engine fan blades. The consequent normal deformation and contact force were determined and presented in Section 5.

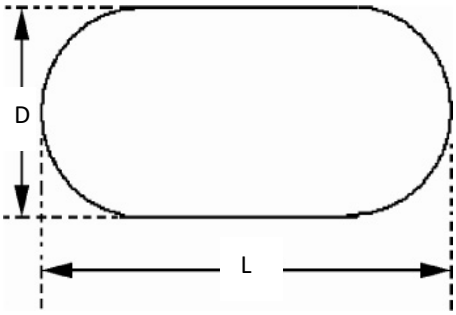

Figure 5 Details of bird's configurations considered

Table 8 Bird dimension parameters (unit: mm).

Bird Category	Length (L): Diameter (D)	Weight
Small	160:56.5	0.34 kg
Medium	244:114	1.80 kg
Large	288:144	3.60 kg

Table 9 Material parameters for bird [51].

Density, ρ	Young's Modulus, E	Poison's ratio, υ	Yield stress, σ_y	Failure stress, σ_f	Failure strain, ε_f
968	10.0 GPa	0.3	0.5 MPa	4.27 MPa	0.0122

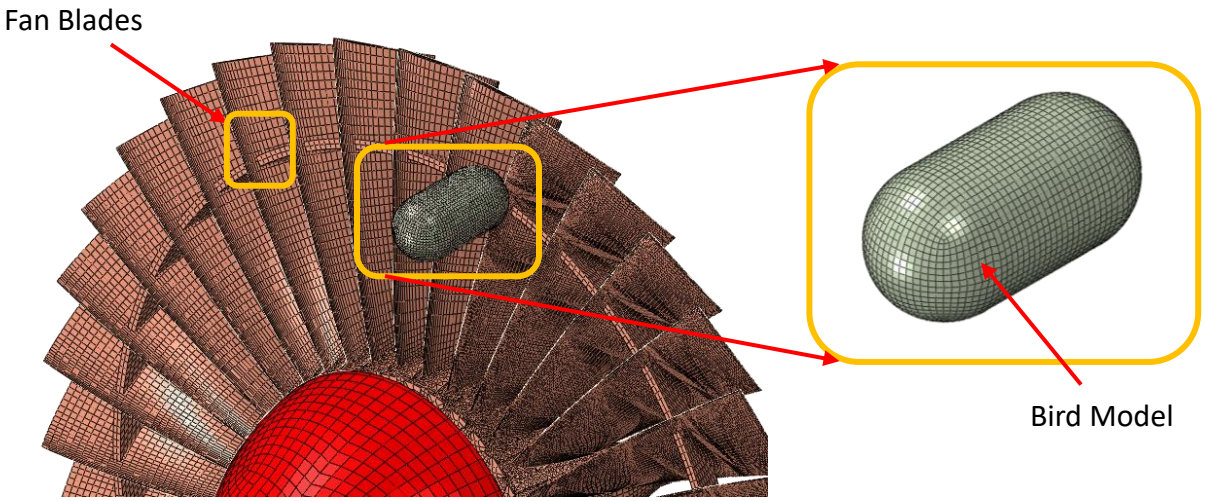

(a) (b)

Figure 6 FEM model for bird ingestion simulation: (a) isometric view of bird-engine assembly model; (b) FEM model of the bird.

4. Validation of Impact Model

Validation of the bird and drone model in FEM simulation is performed before the collision simulation between bird and drone with aircraft engine fan blades take place. This validation is to ensure the material properties for bird and engine fan blades could represent the actual behavior during impact load condition. Two validation models prepared, one is the bird model impacted on to a steel plate and the second validation simulation is the engine fan blades impacted by a steel ball.

4.1. Validation of Bird Impact model

An experiment of bird impact was performed by Lavoie et al. [52] by using a bird impinging onto a square plate. The Rolled Homogeneous Armor (RHA) square steel plate adopted in their experiment had the dimensions of 0.305 m × 0.305 m and a thickness of 0.0127 m. The target plate was attached to the concrete floor and clamped around its boundary over a width of 0.0127 m, and the projectile is impacted at the target perpendicularly with an initial velocity of 100 m/s.

The impact simulation is carried out to compare our simulation with Lavoie's experiment to demonstrate the material used in the collision simulation is sufficient. Figure 7 shows the setup of the bird impact simulation from both the orthographic and lateral views for the bird impact on the square rigid plate. Besides, the interaction between bird and steel plate is defined as a frictionless boundary condition. The deformation of the bird from the simulation is analyzed as well as the bird shape changes from the impact at an angle of 0° as shown in Figure 8. The snapshots are taken at a certain time with every 0.66 ms to show the bird deformation throughout the impact process.

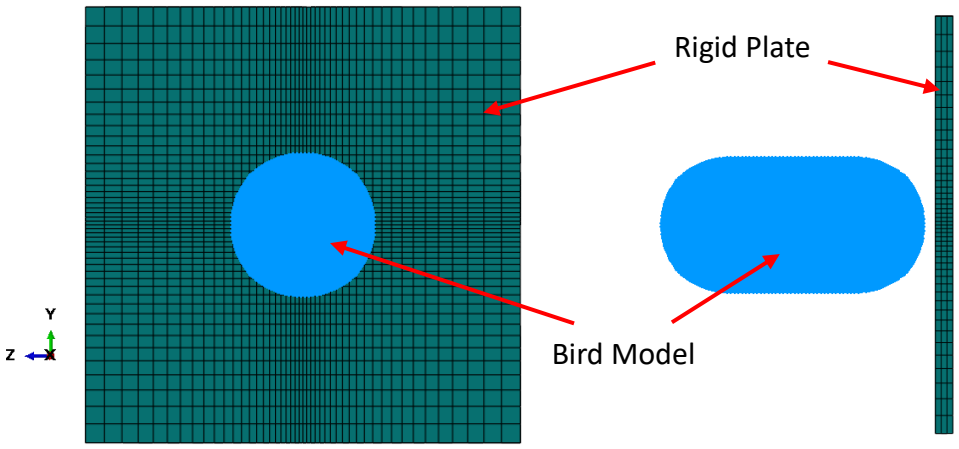

(a) Orthographic view (b) Lateral view

Figure 7 FEM model of bird strike on a plate.

The diameter of the bird projected on the rigid plate was simulated in impact collision (see Figure 9(a)) and compared with the measurement from the camera. It is noted that the bird projection diameter on the rigid plate keep increased from the start of the impact and has stopped when the bird debris has reached the edge of the plate. Moreover, Figure 9(b) shows the impact force from the bird impact. When the bird impinges onto the plate initially, the cylindrical bird has two peaks in the curve, as observed by Jun and Yulong [53]. The good correlation between the experimental and FEM collision simulation results confirms that the SPH setup and its parameters used in the simulation are appropriate.

Experiment[52]	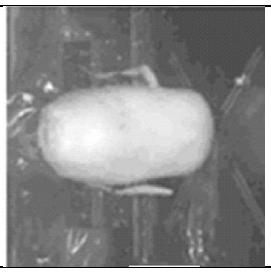		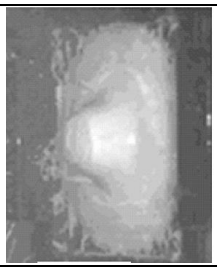	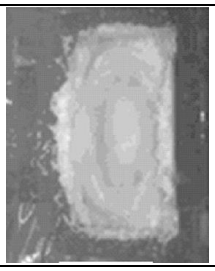
Present Simulation				
	(a) *t*=0.0 ms	(b) *t*=0.66 ms	(c) *t*=1.32 ms	(d) *t*=1.98 ms

Figure 8 The deformation process predicted by experiment and simulation for bird impacting on the plate.

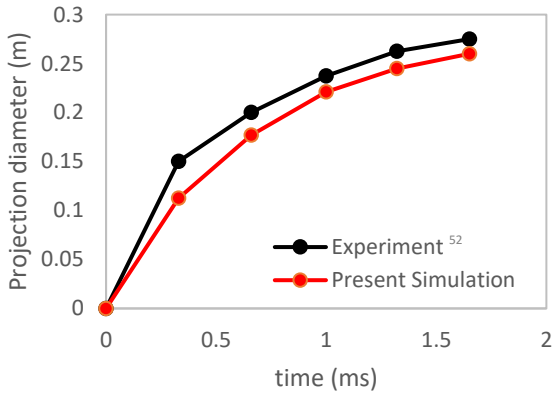

(a) Bird projection diameter.

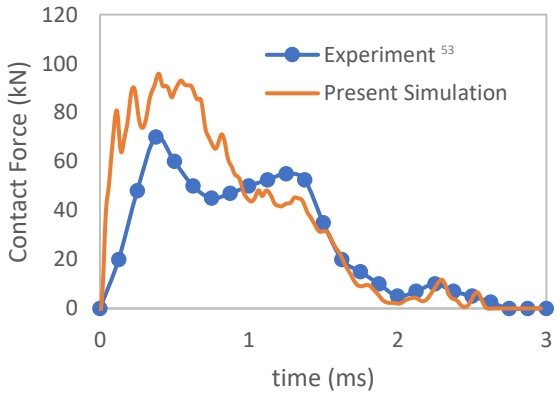

(b) Contact force vs time.

Figure 9 Comparison between simulation and experiment for plate impacted by birds.

4.2. Validation of Engine Fan Blade model

Titanium alloy Ti-6Al-4V is the material widely used in the aerospace industry to manufacture engine components like fan disks, fan blades, and shafts. The fan blades installed in the turbofan aircraft engine are taken as the specimens in this study. To mimic the engine ingestion conditions that might occur in service from ingested particles at high velocities and strain rates, the specimens

are impacted ballistically using 3 mm steel ball projectiles at different impact speeds, as depicted in Figure 10.

The damage of the fan blade is analyzed initially, and in general, the damage depth of the fan blades is enlarged with the increase of the impact speed, as shown in Figure 11. As shown in Figure 11, fan blades damage from the experiment [54] and simulation after an impact velocity of 280 m/s and 100 m/s. A good correlation of damage to fan blades is observed between the experimental and simulation results, illustrating that the material properties definition, Johnson-Cook model, and its setup used in the simulation are appropriate and can be used for the UAV collision simulation.

4.3. Comparison between Drone Collision and Bird Strike

Table 10 shows the damage of fan blades from FEM simulation of bird and drone collision for different weight categories at an impact velocity of 145 knots and engine rotation of 5000 RPM. From the FEM simulations, a small indentation on engine fan blade was observed from both the collision of small drone and small bird category. In addition, the damage of fan blades from the large drone collision was more severe than the medium drone category due to the fracture at the root of the fan blade. It is notable that fractured fan blades can potentially compromise the engine structural integrity and performance (e.g., drone debris or fractured fan blades ingested into engine core may result in thrust loss [55]). Similarly, material loss and fracture damage at the point of collision was detected for bird collision from the medium and large categories, respectively.

Figure 12 and Figure 14 show the deformation process of the drone and bird for the large category at the collision position of 75%. The deformation time for bird collision was observed to be shorter than the drone. This could likely be due to the reduced length and width of the bird when compared to that of the drone. Moreover, a longer deformation time in the drone collisions caused the drone to impact more fan blades. This led to much severe damage to the engine fan blades (fracture of root fan blade).

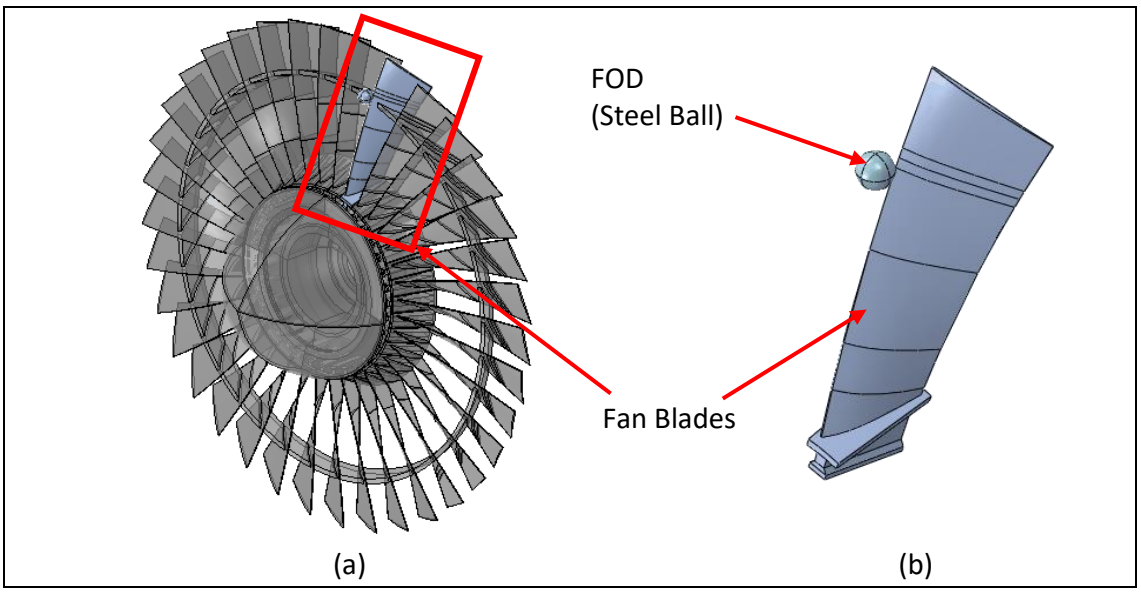

Figure 10 FEM model of the impact orientations for FOD impact test: (a) isometric view of steel ball-engine assembly model; (b) steel ball at the collision position.

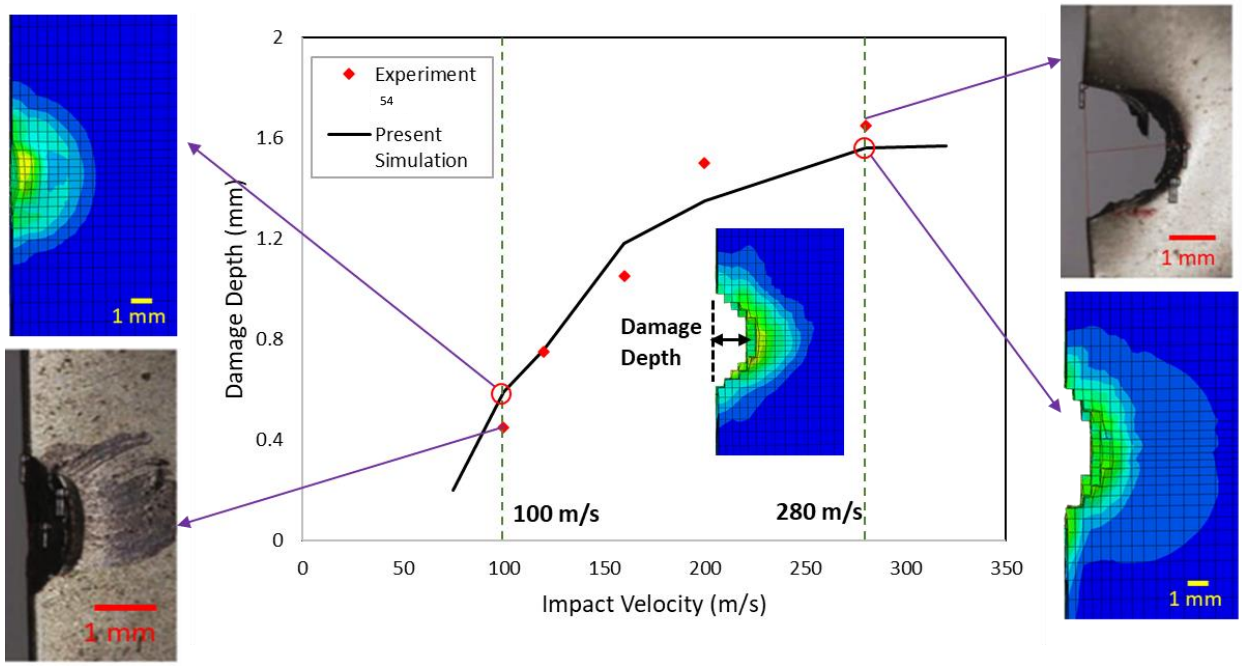

Figure 11 Comparison between the FEM simulation and experiment for the damage depth of fan blades under different impact velocities.

Table 10 Damage of fan blades for bird and drone collisions at collision position of 75% (145 knots and 5000 RPM).

Category*	Drone	Bird
Small	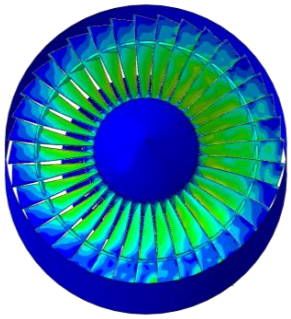	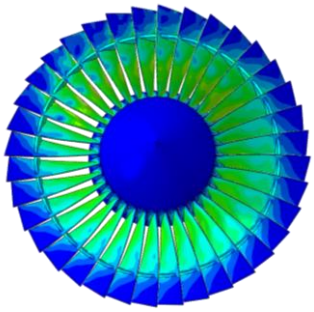
Medium	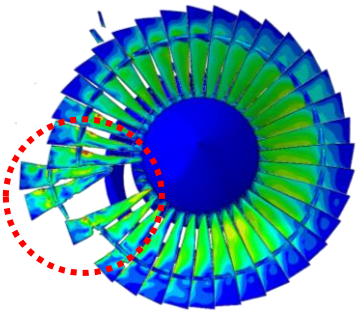	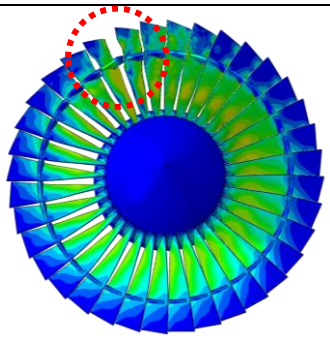
Large	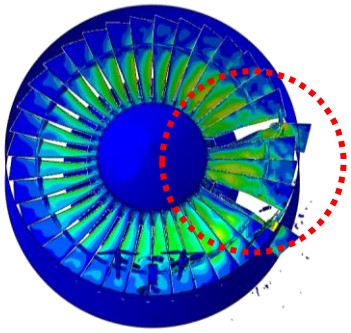	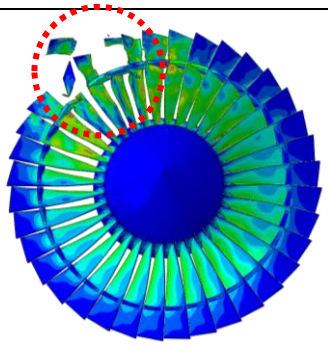

*Refer Table 1 for the wight of bird and drone.

Figure 13 and Figure 15 show the contact force of drone and bird collision for three different categories at the collision position of 75%. The large bird and large drone category have the highest contact force because both have the highest kinetic energy with a contact force of 250 kN and 200 kN, respectively. That is because the drone has a solid body, which is much stiffer than the bird body and will lend to higher localized stress at the impact position. Hence, the drone collision will cause more severe damage to the fan blade than the bird collision.

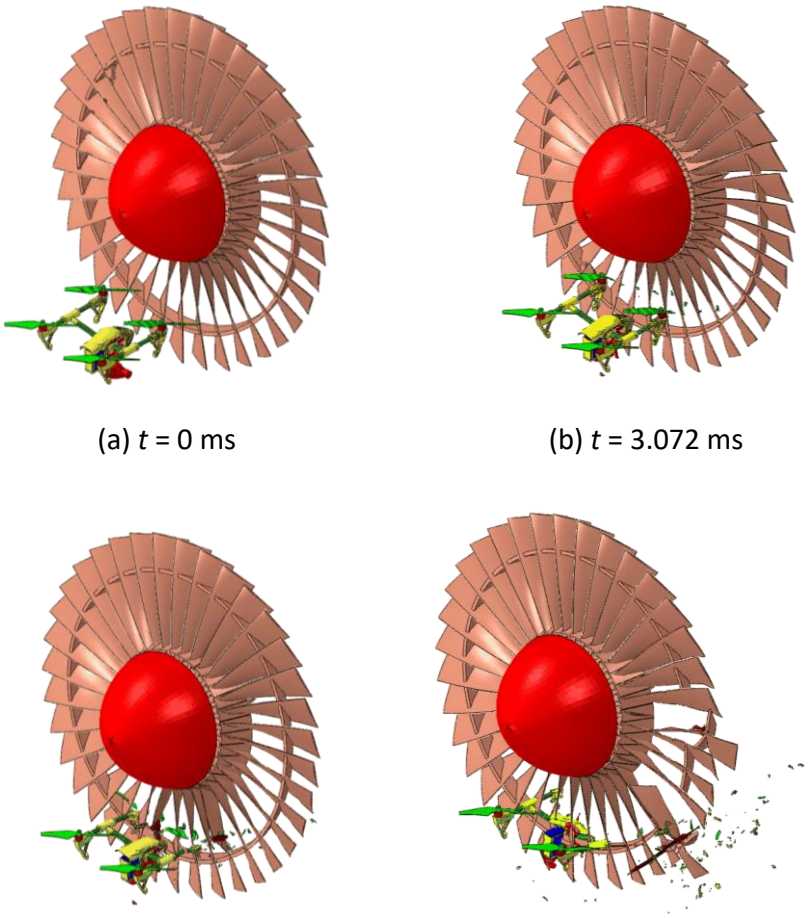

(a) t = 0 ms (b) t = 3.072 ms

(c) t = 4.096 ms (d) t = 5.26 ms

Figure 12 The deformation process of drone collision (large drone, 75% collision position).

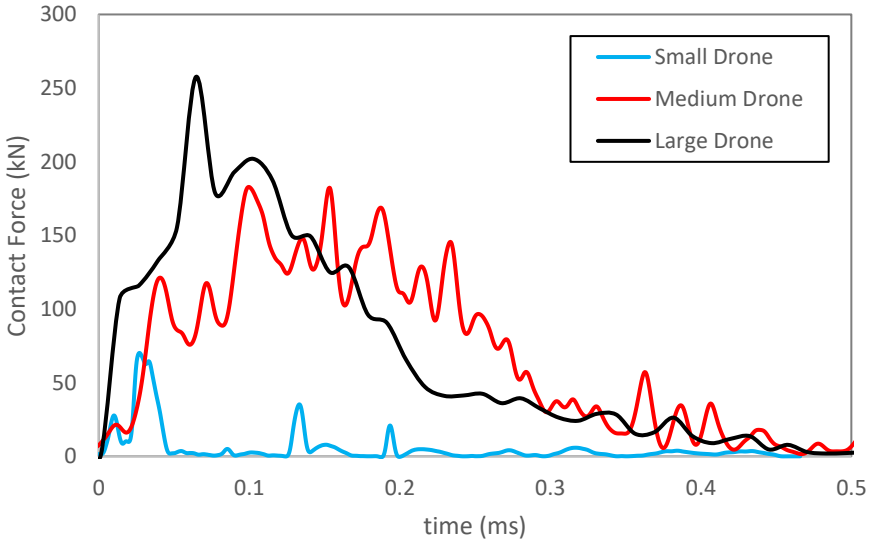

Figure 13 The contact force time history for different drone categories (75% collision position).

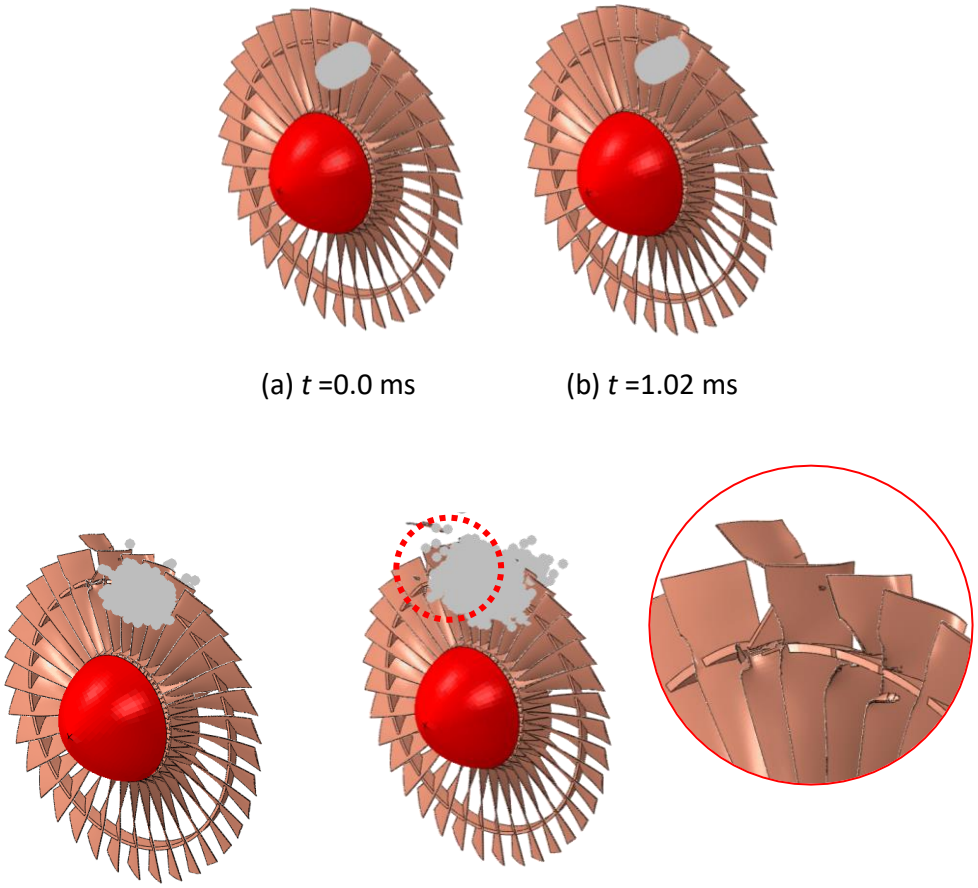

(a) t =0.0 ms (b) t =1.02 ms

(c) t =2.04 ms (d) t =2.56 ms

Figure 14 The deformation process of bird collision (large bird, 75% collision position).

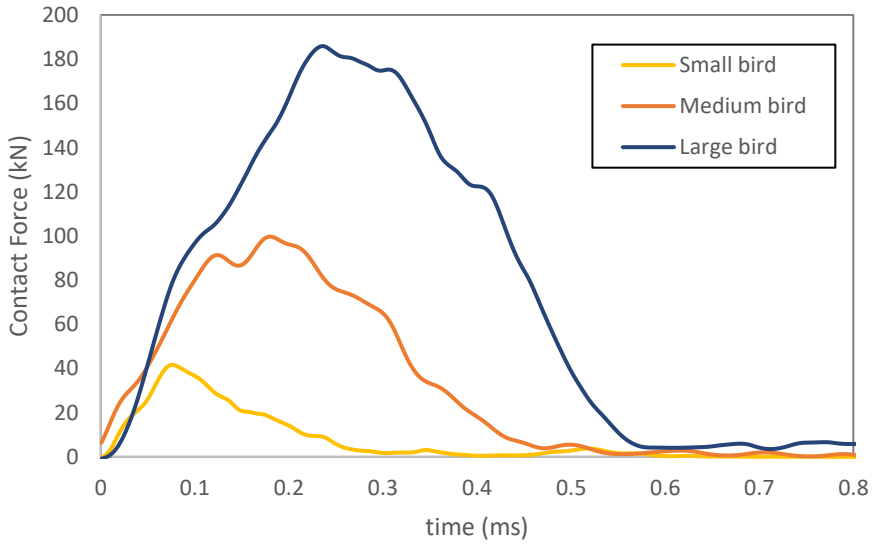

Figure 15 The contact force time history for different bird categories (75% collision position).

5. Results and Discussion

Different simulation parameters will influence the result from the drone ingestion performance; For example, a drone ingested at high impact speed will cause severe damage to a greater number of fan blades compared to a drone ingested at low impact speed. This section is focused on examining the influence of certain impact collision parameters (i.e., impact speed, engine speed rotation) on the fan blades damage and impact force. In addition, damage of engine fan blade due to the impact by different drone categories and vibration of engine fan blades due to impact from the large drone category will also be analyzed.

5.1 Effect of Drone Impact Velocity

Table 11 shows the damage of fan blades from FEM simulation of drone impact for medium drone category under three different impact speeds. It is observed that all three drones' impact velocity at an engine rotation speed of 5000 RPM led to severe damage of fan blades. Moreover, the fracture at the root of the fan blade was witnessed. This phenomenon can potentially compromise the engine structural integrity (e.g., engine vibrate excessively). Similarly, material loss damage and fracture at the impact position was also observed.

Table 11 Medium drone collision at engine rotation 5000RPM for different impact velocity (75% collision position).

(a) 145 kts	(b) 200 kts	(c) 250 kts
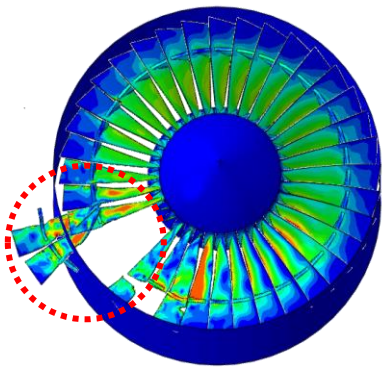	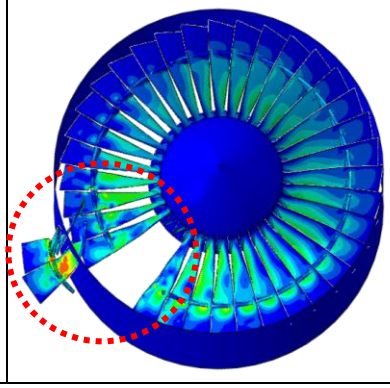	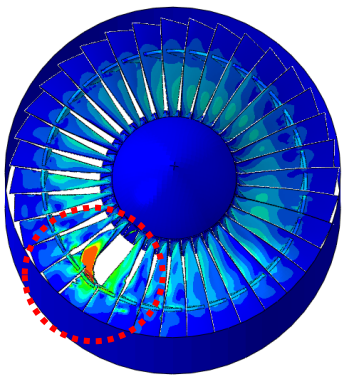

Figure 16 shows the contact force of drone collision for three different impact velocities at the collision position of 75%. The impact velocity of 145 knots had the highest contact force of 294 kN when compared to 126 kN for an impact velocity of 250 knots. This was likely due to the increased

contact time of the drone causing more fan blades to be impacted. Subsequently, this resulted in a higher contact force with a greater number of fan blades being fractured. In contrast, the drone collision at higher impact velocity resulted in a higher localized stress at the impact position [56], larger fan blade bending and lowest contact force.

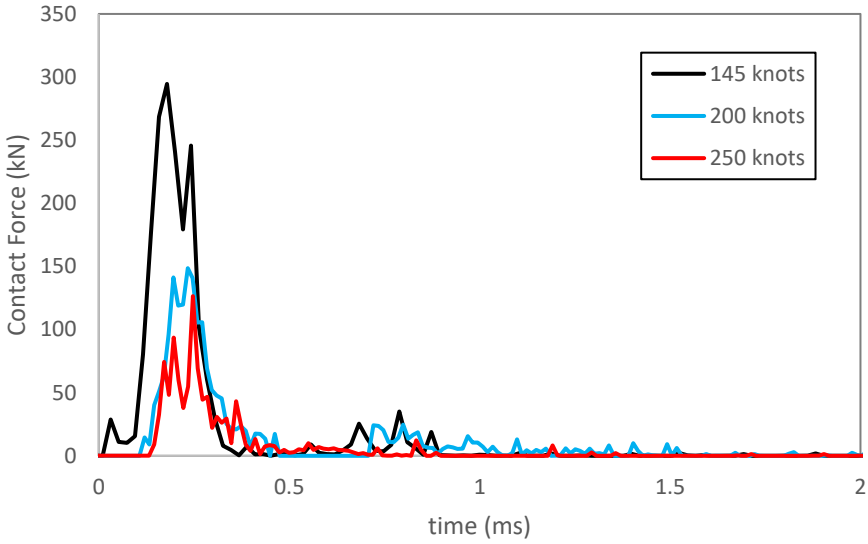

Figure 16 The Contact force time history for medium drone collision at engine rotation of 5000RPM for different impact velocities (75% collision position).

5.2 Effect of Engine Rotation Speed

This sub-section studies the influence of different engine rotation speeds on the fan blades damage for medium drone category. Table 12 depicted the damage of engine fan blades from FEM simulation, it was found that the drone's impact velocity of 145 knots at engine rotation of 4000 RPM and 50000 RPM led to the fracture at the root of the fan blade. This was more severe when compared with the damage at engine rotation of 3000 RPM. For the drone impact at engine rotation of 3000 RPM, minor material loss and fracture at the impact position was observed.

Figure 17 presents the contact force of drone collision for three different engine rotation speeds at the collision position of 75%. The engine rotation speed of 5000 RPM had the highest contact force of 294 kN when compared to that of 115 kN at an engine rotation speed of 3000 RPM. This was due to the engine fan blades experiencing the highest kinetic energy at an engine rotation speed of 5000RPM and resulting in higher localized stress at the drone impact position. This led to higher contact force with severe fan blades damage as compared to lower engine rotation speeds.

Table 12 Medium drone collision at engine rotation of 145 knots for different engine rotation speeds (75% collision position).

(a) 3000 RPM	(b) 4000 RPM	(c) 5000 RPM
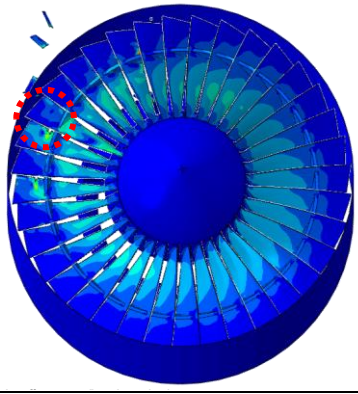	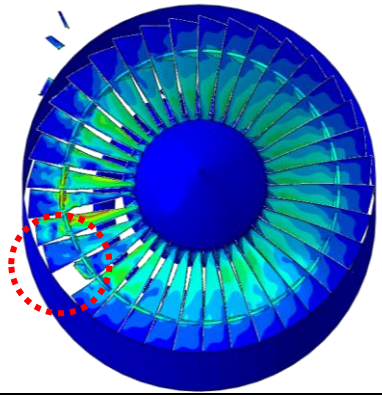	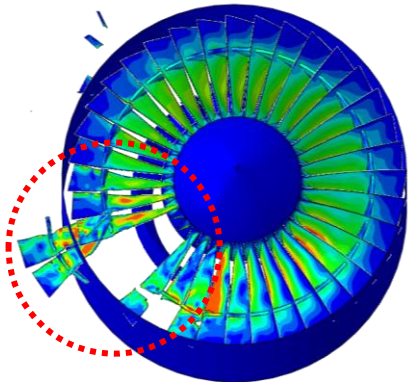

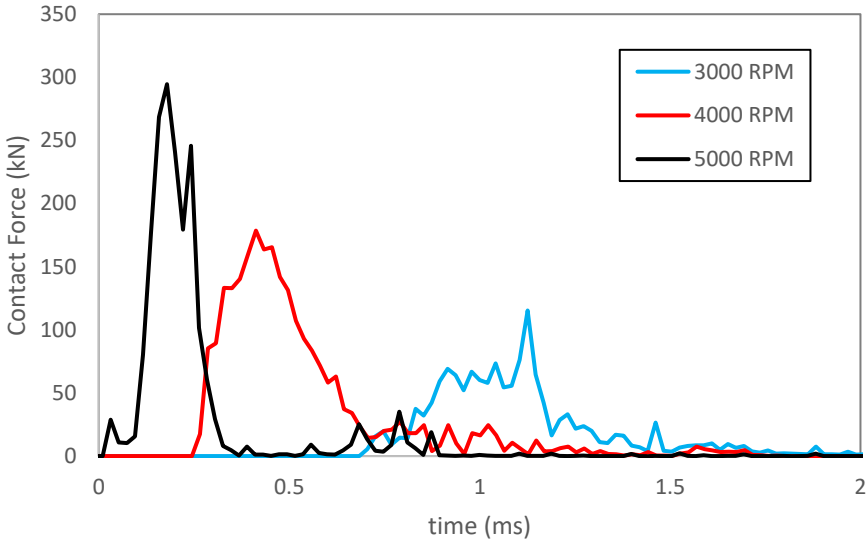

Figure 17 The contact force time history for medium drone at impact velocity of 145 knots for different engine rotation speeds (75% collision position).

5.3 Effect of Collison Position

This sub-section studies the influence of different drone collision position on the damage of fan blades for different drone categories. Table 13 summarizes the damage of engine fan blades under different drone categories at three collision positions. The large drone category can cause fracture damage at the root of the engine fan blades for all collision positions. The same damage can be observed for the collision position of 50% and 75% for the medium drone category, and large bending deformation can be found for the collision position of 25%.

To better understand the damage to fan blades, the plot of contact force for the medium drone category is presented in Figure 18. For the contact force value less than 155 kN, no fracture damage to fan blades is found. It can be concluded that the large drone category (more than 2 kg) can cause severe fan blades damage by comparing to the medium and small drone categories, especially for the collision position of 25% where drone debris can be ingested into and potentially cause damage to the engine core.

Table 13 Damage of the fan blades for the impact of different drone categories and collision positions.

Category	**Collision Position**		
	25%	**50%**	**75%**
Small (<1.5kg)	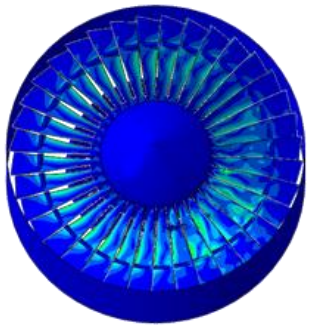	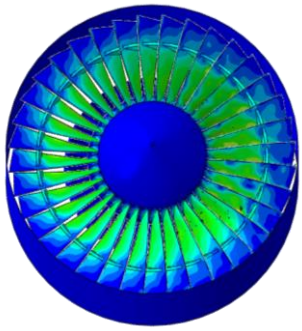	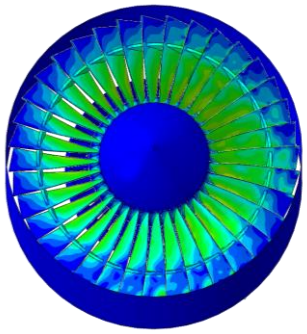
Medium (1.5-3.5 kg)	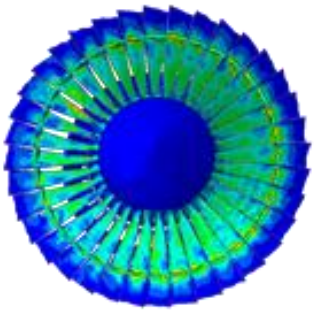	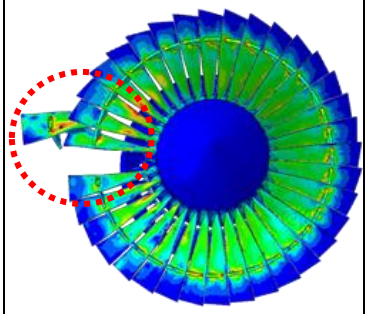	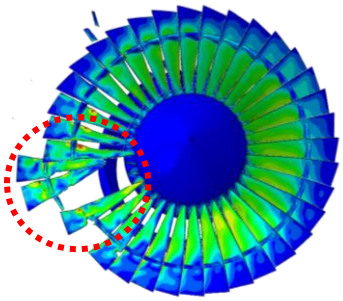
Large (>3.5 kg)	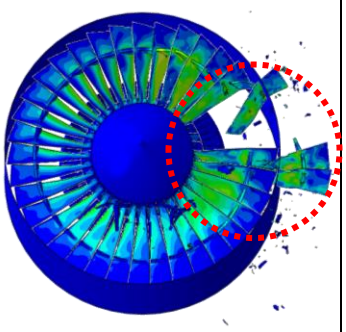	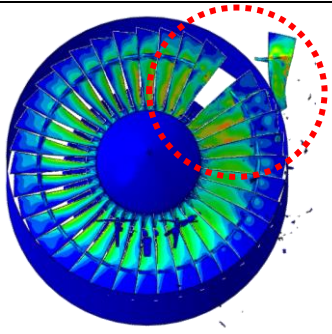	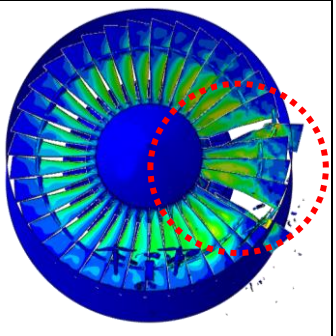

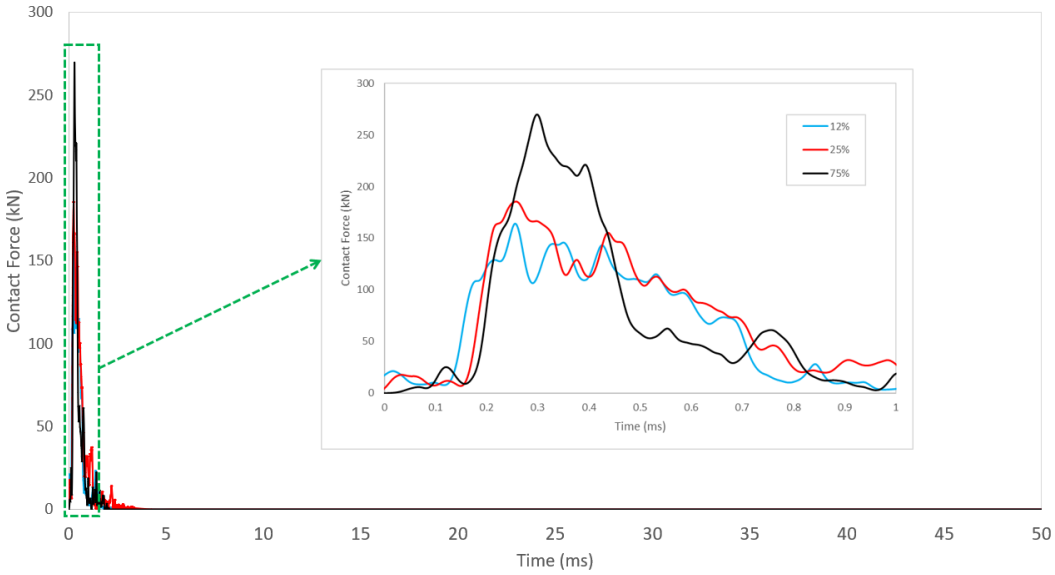

Figure 18 The contact force time history of fan blade at different collision positions (medium drone category).

5.4 Vibration of Fan Blades due to the Drone Impact

Figure 18 shows the time history of contact force during a period of 50 ms, which illustrates that the impact lasts only around 1 ms and the contact force will decrease to about zero after 1 ms. During the impact, the impact force acted on the fan blades leads to the fracture and deflection of fan blades. Then after, the deflected fan blades will continue moving and vibrates over a balance position, which may last over 50 ms, which are depicted in Figure 19. Here, the position of the three fan blades where fan blades deflection from vibration (i.e., displacement) is probed from the FEM simulation. The displacement is taken at Position 1 (P1), Position 3 (P3), Position 4 (P4), and Position 6 (P6) are where the fan blades are unimpacted and unfractured; on the other hand, Position 2 (P2) and Position 5 (P5) are the points that the blade was impacted by drone and fractured at its middle position.

Figure 19(a) and Figure 19(b) show the displacement of engine fan blades at two probe positions at 12.5% and 25% from the root for the total time step of 50 ms. The maximum fan blades displacement for the position 25% is 44.4% at time t_4, which is higher than the position of 12.5%. This result is because the fractured blade case because distance from beam fixed point will have bigger displacement.

5.5. Damage Severity Assessment Matrix

In this sub-section, the result of engine fan blades obtained in section 5.3 is used to establish a damage severity assessment matrix to evaluate the damage level to aircraft safety for different

drone weight categories. The damage severity level for small, medium, and large drone categories under the approach flight phase is summarized in Table 14.

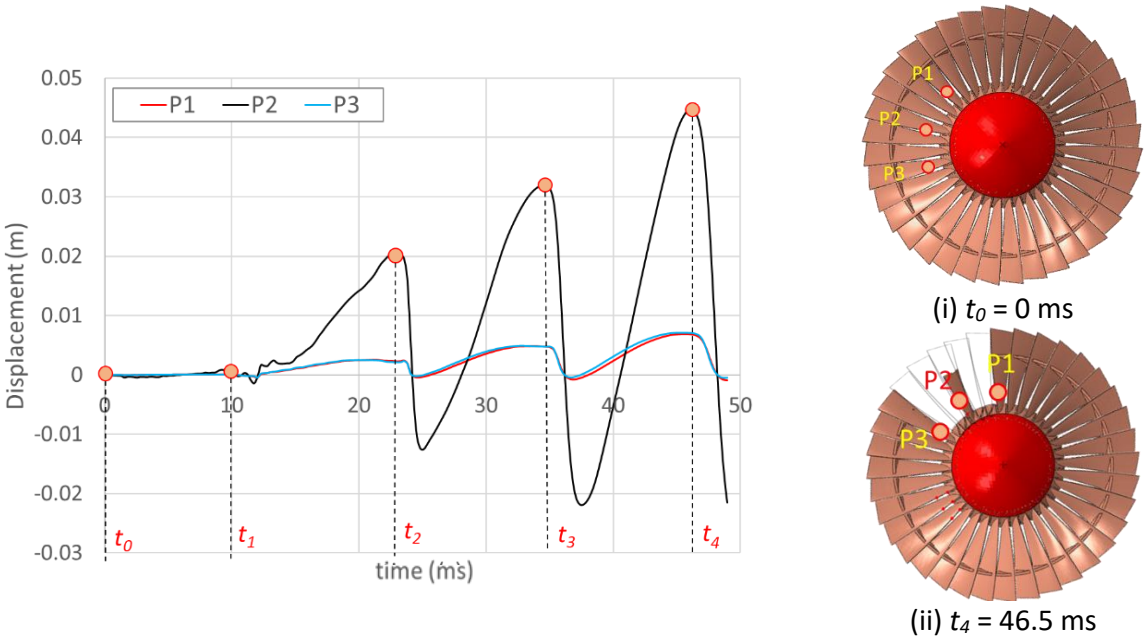

(i) t_0 = 0 ms

(ii) t_4 = 46.5 ms

(a) Collision Position = 25%

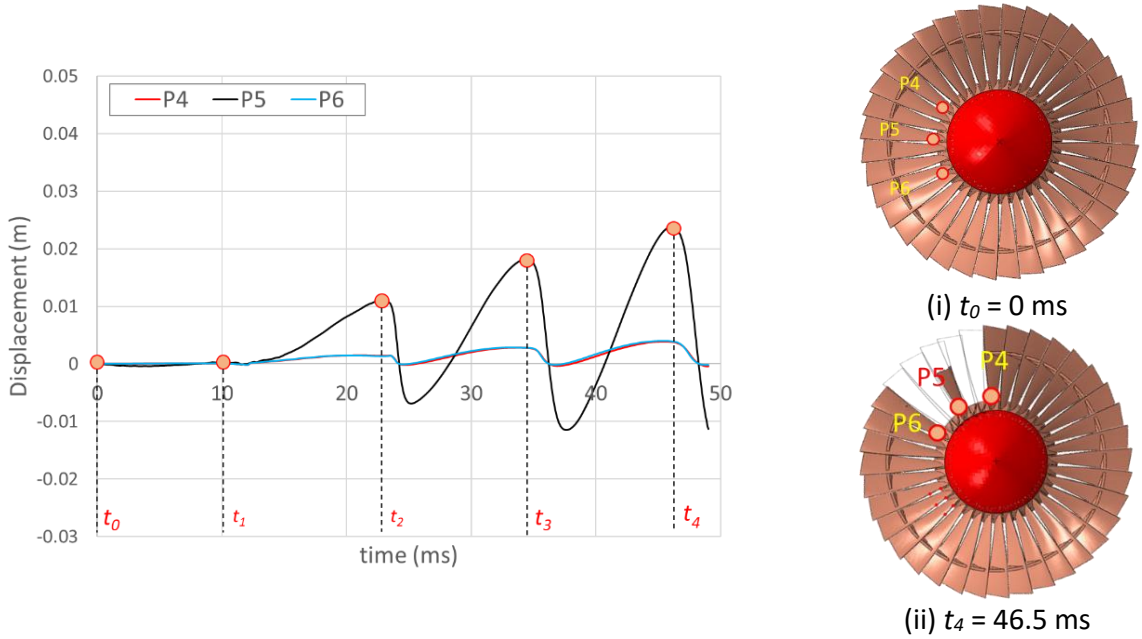

(i) t_0 = 0 ms

(ii) t_4 = 46.5 ms

(b) Collision Position = 12.5%

Figure 19 Plot of the fan blade displacement time history at collision position (a) 25% and (b) 12.5%; (i) and (ii) show the fan blades deformation during the drone ingestion process for (75% collision position).

It is found that the weight of drone plays a significant role in the damage of fan blades where damage severity level for the large drone categories is defined as level 4 due to the significant damage (broken) to engine fan blades for collision position of 25% compared to small and medium drone categories which are defined as level 1 and level 3, respectively.

Table 14 Damage Severity assessment matrix for the drone collision.

Drone Category	Collision Position	Damage Level	Damage Descriptions
Small (<1.5kg)	25%	Level 1	• No significant damage to the fan blade (e.g., small indentation).
	50%	Level 2	• Slight damage to the fan blade (e.g., small bending or small material loss).
	75%	Level 2	• Slight damage to the fan blade (e.g., small bending or small material loss).
Medium (1.5-3.5 kg)	25%	Level 3	• Damage to fan blade (e.g., large bending, large material loss or tear).
	50%	Level 4	• Severe damage to fan blade (e.g., Fan blade fractured, windmill).
	75%	Level 4	• Severe damage to fan blade (e.g., Fan blade fractured, windmill).
Large (>3.5 kg)	25%, 50%, 75%	Level 4	• Severe damage to fan blade (e.g., Fan blade fractured, windmill).

The collision position will also influence damage severity level; for example, for the small drone category, the damage severity level of 25% impact position case is defined as level 1, while for collision positions, 50% and 75% are defined as level 2 because the damage (small bent and material loss) to fan blades can be observed. The same case can be observed for the medium drone category, where damage level 3 is defined for the impact position 25%, which will result in damage to fan blades (large material loss and large bending). Besides, damage level 4 is obtained for 50% and 75% impact positions as significant damages (broken) of fan blades are found. Although damage level 4 is defined for the large drone category regardless of collision position, significant damages (broken) at the root of fan blades are found.

6. Conclusion

This work presents a comparative study on the damage of engine fan blades under bird strike and small drone collision with three different weight categories. The small, medium, and large size (dimensions) drones are considered to have the same mass equivalent to bird strike certification requirements. From this study, the following conclusion can be drawn:

1. The impact velocity of 145 knots and engine rotation speed of 5000 RPM for the drone collision is found to cause more severe damage to engine fan blades, wherein the fracture at the root of fan blades can be found by comparing to the damage under the bird strike. It was found for the same impact velocity at the lowest engine rotation speed (3000 RPM) shows damage severity of level 2 where only small material loss of the engine fan blades are found.
2. The drone with a weight higher than 1500 g (large and medium drone) produces the highest level of damage (level 4), where broken fan blades can be found at a collision position of 50% and 75% because the highest contact force is generated from this collision. The collision severity level for the drone small than 250 g is mostly defined as level 2 and level 1 due to the slight damage of fan blades.
3. On the other hand, the impact position of the drone also plays an essential role in the collision severity level. The damage level of fan blades is the largest for the impact position of 75%, followed by the positions 50% and 25%. The damage at the collision position lower than 50% may lead to debris ingested into the engine core and further damage internal engine structure like LPC and HPC. A study done in reference [55] shows that the collision of a medium drone category at an impact position of 25% may not cause damage to the engine fan blades. However, it will also risk the aircraft operation because the drone's debris may be ingested into the engine core and inflict damage to compressor blades, leading to an engine thrust loss.

Results from this study demonstrated that damage to the fan blade from a large bird collision caused fracture at the point of impact and potentially compromise the engine structural integrity and its performance. In contrast, drone collision for medium and large categories led to fracture at the root of fan blades. This may lead to more severe damage and might similarly compromise overall engine structural integrity. Hence, it is likely that drone strike certification may have to be considered for future engine certifications with the increase in drone threats and operations. Since drone

collisions might cause vibration to rotating blades of the engine, the method of frequency equation derivation can also be applied together with the FEM simulation[57, 58] of aircraft engines.

Acknowledgement

This research is supported by the Civil Aviation Authority of Singapore and the Nanyang Technological University, Singapore under their collaboration in the Air Traffic Management Research Institute. Any opinions, findings, and conclusions or recommendations expressed in this material are those of the authors and do not reflect the views of the Civil Aviation Authority of Singapore.

References

1. Jenkins D and Vasigh B. *The economic impact of unmanned aircraft systems integration in the United States*. Association for Unmanned Vehicle Systems International (AUVSI), 2013.
2. Wang CHJ, Tan SK and Low KH. Three-dimensional (3D) Monte-Carlo modeling for UAS collision risk management in restricted airport airspace. *Aerospace Science and Technology*. 2020; 105: 105964.
3. Gregory K. London's Gatwick Airport reopens; drone suspects questioned (Retrieved 25 December 2018.). *The Salt Lake Tribune*. 2018.
4. Hauck C and Geis J. Air Mines: Countering the Drone Threat to Aircraft. *Air & Space Power Journal*. 2017: 26-40.
5. Belcastro CM, Newman RL, Evans J, Klyde DH, Barr LC and Ancel E. Hazards identification and analysis for unmanned aircraft system operations. *17th AIAA Aviation Technology, Integration, and Operations Conference*. 2017, p. 3269.
6. Sedaghat-Pisheh H, Rivera AR, Biaz S and Chapman R. Collision avoidance algorithms for unmanned aerial vehicles using computer vision. *Journal of Computing Sciences in Colleges*. 2017; 33: 191-7.
7. Civail Aviation Authority. Drone Safety Risk: An assessment CAP 1627. 2018.
8. Pernas-Sánchez J, Artero-Guerrero J, Varas D and Lopez-Puente J. Artificial bird strike on Hopkinson tube device: experimental and numerical analysis. *International Journal of Impact Engineering*. 2019: 103477.
9. Riccio A, Cristiano R, Saputo S and Sellitto A. Numerical methodologies for simulating bird-strike on composite wings. *Composite Structures*. 2018; 202: 590-602.

10. Cerquaglia ML, Deliége G, Boman R, Papeleux L and Ponthot JP. Reprint of: The particle finite element method for the numerical simulation of bird strike. *International Journal of Impact Engineering*. 2017; 110: 72-84.
11. Metz IC, Ellerbroek J, Mühlhausen T, Kügler D and Hoekstra JM. The Bird Strike Challenge. *Aerospace*. 2020; 7: 26.
12. Kim D-H and Kim S-W. Evaluation of bird strike-induced damages of helicopter composite fuel tank assembly based on fluid-structure interaction analysis. *Composite Structures*. 2019; 210: 676-86.
13. Heimbs S. Computational methods for bird strike simulations: A review. *Computers & Structures*. 2011; 89: 2093-112.
14. Dolbeer RA, Wright SE, Weller J, Anderson AL and Begier MJ. Wildlife strikes to civil aircraft in the United States, 1990-2014. 2015.
15. Zhang Z, Li L and Zhang D. Effect of arbitrary yaw/pitch angle in bird strike numerical simulation using SPH method. *Aerospace Science and Technology*. 2018; 81: 284-93.
16. Yu Z, Xue P, Yao P and Zahran MS. Analytical determination of the critical impact location for wing leading edge under birdstrike. *Latin American Journal of Solids and Structures*. 2019; 16: e152.
17. Di Caprio F, Cristillo D, Saputo S, Guida M and Riccio A. Crashworthiness of wing leading edges under bird impact event. *Composite Structures*. 2019; 216: 39-52.
18. Hu D, Song B, Wang D and Chen Z. Experiment and numerical simulation of a full-scale helicopter composite cockpit structure subject to a bird strike. *Composite Structures*. 2016; 149: 385-97.
19. Dar UA, Awais M, Mian HH and Sheikh MZ. The effect of representative bird model and its impact direction on crashworthiness of aircraft windshield and canopy structure. *Proceedings of the Institution of Mechanical Engineers, Part G: Journal of Aerospace Engineering*. 2019; 233: 5150-63.
20. SKYBrary. Aircraft Certification for Bird Strike Risk. August 2020.
21. Charles L, Kelly C and Vicente G. Simulation of Aircraft Engine Blade-Out Structural Dynamics. 2001.
22. Frank J. Complicated Analysis More research needed into potential drone–manned aircraft impact severity. February 2018.
23. Olivares G, Gomez L, Espinosa de los Monteros J, Baldridge RJ, Zinzuwadia C and Aldag T. Volume II–UAS Airborne Collision Severity Evaluation–Quadcopter. 2017.
24. Olivares G, Lacy T, Gomez L, et al. Volume III–UAS Airborne Collision Severity Evaluation–Fixed-Wing. 2017.

25. Lu X, Liu X, Li Y, Zhang Y and Zuo H. Simulations of airborne collisions between drones and an aircraft windshield. *Aerospace Science and Technology*. 2020; 98: 105713.
26. Kiran D'Souza, Troy Lyons, Thomas Lacy and Kota KR. Volume IV – UAS Airborne Collision Severity Evaluation – Engine Ingestion. August 2017.
27. International Bird Strike Committee (IBSC). Best Practices Manual An Aviation Guide To The Management Of Wildlife Hazards. 2002.
28. Dukiya JJ and Gahlot V. An Evaluation of the Effect of Bird Strikes on Flight Safety Operations at International Airport. *International Journal for Traffic and Transport Engineering*. 2013.
29. Dukiya JJ and Ahmad A. Aircraft flight safety and birds strikes management in Aminu Kano International Airport, Nigeria. *Advancement in Scientific and Engineering Research*. June 2014; 2: 12.
30. Holbech LH, Asamoah A and Owusu EH. A rapid assessment of species-specific bird strike risk at the Kotoka International Airport in Accra, Ghana. *Ostrich*. 2015: 9.
31. Liu H, Che Man MH, Ng BF and Low KH. Airborne Collision Evaluation between Drone and Aircraft Engine: Effects of Position and Posture on Damage of Fan Blades. *AIAA AVIATION 2020 FORUM*. 2020.
32. Che Man MH, Liu H, Ng BF and Low KH, "Preliminary Evaluation of Thrust Loss in Commercial Aircraft Engine due to Airborne Collision with Unmanned Aerial Vehicles (UAVs)," *2020 International Conference on Unmanned Aircraft Systems (ICUAS)*, 2020, doi: 10.1109/ICUAS48674.2020.9214048.
33. Systemes Dassault. ABAQUS 6.14 User's Guide. 2014.
34. European Aviation Safety Agency (EASA). Certification specifications and acceptable means of compliance for engines. 2018.
35. European Aviation Safety Agency (EASA). EASA Drone Collision Task Force. *European Aviation Safety Agency*. 2016: 1-33.
36. Dennis N and Lyle D. Bird Strike Damage & Windshield Bird Strike. 2009: 181.
37. European Aviation Safety Agency (EASA). Bird Strike Damage & Windshield Bird Strike: Final Report. 2009.
38. European Aviation Safety Agency (EASA). Type-Certificate Datasheet: for AIRBUS A318-A319-A320-A321. 2015.
39. Administration USDoTFA. Continuous Descent Final Approach. January 2011.
40. Hovey PW, Skinn DA and Wilson JJ. Engine Bird Ingestion Experience of the Boeing 737 Aircraft – Expanded Data Base (October 1986 – September 1989). 1992.

41. D'Souza K, Lyons T, Lacy T and Kota KR. Volume IV–UAS Airborne Collision Severity Evaluation–Engine Ingestion. 2017.
42. Kwon CW, Cheon SE, Song JM, et al. Characteristics of a lithium-polymer battery based on a lithium powder anode. *Journal of Power Sources*. February 2001; 93: 6.
43. Wang T, Qin Q, Wang M, et al. Blast response of geometrically asymmetric metal honeycomb sandwich plate: Experimental and theoretical investigations. *International Journal of Impact Engineering*. 2016.
44. Azom. AISI 4340 Alloy Steel (UNS G43400). Sept 2012.
45. Meng X, Sun Y, Yu J, et al. Dynamic response of the horizontal stabilizer during UAS airborne collision. *International Journal of Impact Engineering*. 2019; 126: 50-61.
46. Johnson GR and Cook WH. Fracture characteristic of three metals subjected to various strains, strain rates, temperatures and pressures. *Engineering Fracture Mechanics*. 1985: 18.
47. Institute BM. Metallic Materials Properties Development and Standardization (MMPDS). July 2016.
48. International CFM. Training Manual CFM56-5B Basic Engine. December 2000.
49. Beardmore R. Tribology_Index Friction Factors. 2020.
50. Uzair AD and Weihong Z. Polymer based aerospace structures under high velocity impact applications; experimental, constitutive and finite element analysis. *Journal of Mechanical Science and Technology*. 2015; 29: 7.
51. Uzair A, Wang J, Xu Y and Zhang W. High-speed Bird Impact Analysis of Aircraft Windshield by Using a Nonlinear Viscoelastic Model. *Applied Mechanics and Materials*. 2013; 290: 6.
52. Lavoie MA, Gakwaya A and Nejad Ensan M. Bird's substitute tests results and evaluation of available numerical methods. *International Journal of Impact Engineering*. 2009; 36: 12.
53. Liu J and Li Y. Numerical simulation of a rotary engine primary compressor impacted by bird. *Chinese Journal of Aeronautics*. 2013; 26: 9.
54. Yu X, Li C, Chang S, Xuan C and Peiyuan L. Foreign Object Damage Performance and Constitutive Modeling of Titanium Alloy Blade. *International Journal of Aerospace Engineering*. 2020; 10.
55. Liu H, Che Man MH and Low KH. UAV airborne collision to manned aircraft engine: Damage of fan blades and resultant thrust loss. *Aerospace Science and Technology*. 2021; 113: 106645.
56. Sivakumar AK, Che Man MH, Liu H and Low KH. " Collision Severity Evaluation of Generalized Unmanned Aerial Vehicles (UAVs) Impacting on Aircraft Engines" *2021 International Conference on Unmanned Aircraft Systems (ICUAS)*, 2021, doi: 10.1109/ICUAS51884.2021.9476872.

57. Low KH, On the methods to derive frequency equations of beams carrying multiple masses. *International Journal of Mechanical Sciences*. 2001; 43: 871-881. DOI: 10.1016/S0020-7403(00)00052-7.
58. Low KH, Eigen-analysis of a tip-loaded beam attached to a rotating joint. *ASME Journal Vibration and Acoustics*. 1990; 112: 497-500. DOI: 10.1115/1.2930134.